# Signals in Solid-State Photochemically Induced Dynamic Nuclear Polarization Recover Faster Than Signals Obtained with the Longitudinal Relaxation Time

**Anna Diller,[†] Shipra Prakash,[†] A. Alia,[†] Peter Gast,[‡] Jörg Matysik,*[,†] and Gunnar Jeschke[§]**

*Leiden Institute of Chemistry, Leiden University, PO Box 9502, 2300 RA Leiden, The Netherlands, Leiden Institute of Physics, Leiden University, PO Box 9504, 2300 RA Leiden, The Netherlands, and Physikalische Chemie, Universität Konstanz, 78457 Konstanz, Germany*

*Received: March 28, 2007; In Final Form: June 16, 2007*

During the photocycle of quinone-blocked photosynthetic reaction centers (RCs), photochemically induced dynamic nuclear polarization (photo-CIDNP) is produced by polarization transfer from the initially totally electron polarized electron pair and can be observed by $^{13}C$ magic-angle spinning (MAS) NMR as a strong modification of signal intensities. The same processes creating net nuclear polarization open up light-dependent channels for polarization loss. This leads to coherent and incoherent enhanced signal recovery, in addition to the recovery due to light-independent longitudinal relaxation. Coherent mixing between electron and nuclear spin states due to pseudosecular hyperfine coupling within the radical pair state provides such a coherent loss channel for nuclear polarization. Another polarization transfer mechanism called differential relaxation, which is based on the long lifetime of the triplet state of the donor, provides an efficient incoherent relaxation path. In RCs of the purple bacterium *Rhodobacter sphaeroides* R26, the photochemical active channels allow for accelerated signal scanning by a factor of 5. Hence, photo-CIDNP MAS NMR provides the possibility to drive the NMR technique beyond the $T_1$ limit.

## 1. Introduction

Due to the small energy splitting of the Zeeman effect, all magnetic resonance methods are intrinsically low in signal sensitivity compared to optical spectroscopic methods. Despite magic-angle spinning (MAS), this problem provides a serious limitation especially in solid-state NMR as lines are broadened by strong dipolar effects. Hence, methods for signal enhancement are of great importance for MAS NMR. Therefore, techniques such as dynamic nuclear polarization (DNP),[1,2] optical pumping,[3,4] and photochemically induced dynamic nuclear polarization (photo-CIDNP)[5,6] currently receive great attention. Those methods rely on the introduction of non-Boltzmann nuclear spin states by using radio frequency or optical transitions. Another strategy to increase the signal is based on enhancement of the experimental cycle frequency by acceleration of re-equilibration. In normal NMR experiments, the kinetics of equilibrium recovery is dominated by nuclear relaxation processes, which are described phenomenologically by the Bloch equations.[7] In particular, the spin−lattice relaxation time $T_1$ provides the kinetics of the development toward the Boltzmann equilibration of a particular nuclear spin system interacting thermally with its surroundings. After the system has regained its Boltzmann polarization, it is ready to be probed by a new NMR experiment. For aromatic $^{13}C$ nuclei in frozen proteins, typical $T_1$ relaxation rates are around some 10 s. Enhanced recovery has recently been shown for protons in liquid NMR by selective enhancement of a subset of protons, while leaving all other protons undisturbed.[8,9] Using $^{13}C$ MAS NMR, heating of polymer samples to the melt state has recently been shown to allow for strong shortening of cycle delay and, hence, experimental time.[10]

In the present publication we investigate the effect of $^{13}C$ photo-CIDNP in the solid state on the recovery rate of the signal. The solid-state photo-CIDNP effect was observed for the first time in 1994 in bacterial photosynthetic reaction centers (RCs) as strong modification of NMR intensities of signals from the electron donor and primary electron acceptor.[11] Recently, enhancement factors above 1000 (at 9.4 T) and 10000 (at 4.7 T) have been observed.[12,13] Upon light excitation, RCs undergo charge separation and transfer an electron from the primary electron donor P to the acceptor side, forming an intermediate radical pair (for review, see ref 14). Due to spin conservation, the radical pair is created in a pure singlet state. This highly ordered non-Boltzmann spin structure is a noneigenstate of the electron pair. In RCs of purple bacteria, the donor is a bacteriochlorophyll (BChl) dimer, called special pair,[12,15] while in the RC of photosystem II of plants, the donor appears to be a chlorophyll (Chl) monomer.[16,17] The solid-state photo-CIDNP effect has been explained[5,12,13] by a combination of three parallel-spin chemical processes in which the two electrons interact with nuclei by hyperfine interaction (Figure 1). In all cases the interaction breaks the symmetry between alpha and beta nuclear spins and net nuclear polarization is created: (i) In the electron−electron−nuclear three-spin mixing (TSM) the symmetry of the coherent spin evolution in the correlated radical pair is broken by state mixing due to electron−electron coupling and pseudosecular hyperfine coupling.[18] (ii) In the differential decay (DD) mechanism, the symmetry of the coherent spin evolution in the correlated radical pair is broken by different lifetimes of singlet and triplet radical pairs.[19] (iii) Due to the absence of a carotene in R26 RCs, the donor triplet lifetime is as long as 100 $\mu$s and thus allows for relaxation due to fluctuating hyperfine fields. In this differential relaxation (DR)

* To whom correspondence should be addressed. E-mail: j.matysik@chem.leidenuniv.nl. Phone: +31-71-527-4198. Fax: +31-71-527-4603.
[†] Leiden Institute of Chemistry.
[‡] Leiden Institute of Physics.
[§] Universität Konstanz.

10.1021/jp072428r CCC: $37.00 
Published on Web 08/16/2007

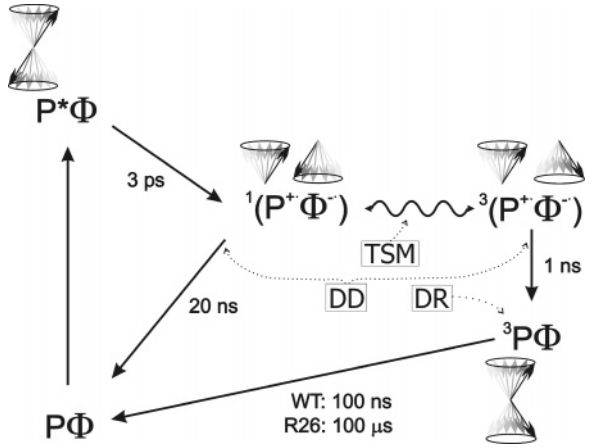


**Figure 1.** Kinetics and spin dynamics of the light-induced electron transport in quinone-blocked RCs of the carotenoid-less strain R26 of *Rb. sphaeroides*. After light absorption, from the photochemically excited state of the primary donor P*, an electron is transferred to the primary acceptor Φ, a bacteriopheophytin cofactor. This initial singlet radical pair $^1(P^{+\bullet}\Phi^{-\bullet})$ is fully *electron* polarized, i.e., created in a state of two-spin order. An electron back-transfer leads to the initial electronic ground state. Due to hyperfine interaction with nuclei, the singlet radical pair evolves into a triplet radical pair $^3(P^{+\bullet}\Phi^{-\bullet})$. Concomitantly to this process of spin intersystem crossing, electron polarization is transferred to nuclei by the TSM, which depends on the difference in *g*-values between the two electrons $\Delta g$, the secular part of the anisotropic hf interaction *A*, and the electron−electron coupling *d*. In the DD mechanism, a net photo-CIDNP effect is caused if spin-correlated radical pairs have different lifetimes in their singlet and triplet states. In RCs having a long lifetime of the donor triplet, as in R26 RCs, the differential relaxation mechanism occurs since nuclear spin relaxation is significant on the triplet branch causing incomplete cancellation of nuclear polarization of both branches.

mechanism, net nuclear polarization is created by selective drain of nuclear polarization created in the triplet radical pair in a long-lived donor triplet state.[20,21] The data presented here demonstrate that photo-CIDNP not only enhances NMR sensitivities but also increases the recovery rate.

## 2. Experimental Section

**Preparation of Bacterial Reaction Centers.** The RCs from *Rb. sphaeroides* wildtype (WT) and R26 were isolated by the procedure of Feher and Okamura.[22] Removal of $Q_A$ was achieved by incubating the RCs at a concentration of 0.6 $\mu$M in 4% LDAO, 10 mM *o*-phenanthroline, 10 mM Tris buffer, pH 8.0, for 6 h at 26 °C, followed by washing with 0.5 M NaCl in 10 mM Tris buffer, pH 8.0, containing 0.025% LDAO and 1 mM EDTA.[23] Approximately 5 mg of the RC protein complex embedded in LDAO micelles was used for NMR measurements.

**Preparation of Samples on Glass Disks.** Bacterial RCs R26 were incorporated into L-α-phosphatidylcholine (egg, chicken; obtained from Avanti Polar-Lipids, Inc., Alabama) bilayers. The lipid/protein weight ratio was approximately 1:1. Drops of about 22 $\mu$L containing around 0.38 mg of protein were spread onto round, 0.1 mm thin glass plates with a diameter of 5.4 mm (Marienfeld GmbH, Lauda-Königshofen, Germany) according to the procedure described.[24,25] The disks were mounted into clear 7 mm sapphire MAS rotors and rehydrated.

**MAS NMR Measurements.** Nonoriented RCs embedded in LDAO micelles were loaded into a 4 mm sapphire MAS rotor. Experiments were done at a spinning frequency of 8 kHz. RC samples loaded on glass disks were mounted into a 7 mm sapphire rotor and measured at a MAS frequency of 4 kHz. The NMR experiments have been performed at 230−240 K,

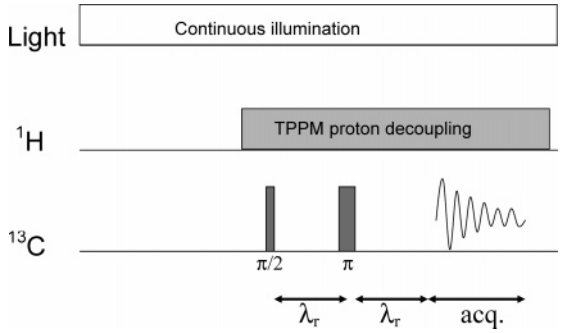


**Figure 2.** MAS NMR pulse sequence applied for obtaining the signal-to-noise factor for various cycle delays at constant experimental time: $\lambda_r$, rotor period; acq., acquisition time. For details, see text.

using DMX-200 and DMX-400 NMR spectrometers (Bruker-Biospin GmbH, Karlsruhe, Germany) equipped with dual-resonance MAS illumination probes.[6] All spectra have been collected using simple $^{13}$C Bloch decay with Hahn echo and detection under two-pulse phase modulation proton decoupling (Figure 2).[26] The sample was frozen under slow spinning (∼600 Hz) to ensure a homogeneous sample distribution against the rotor wall.[27] Each MAS NMR spectrum providing a data point was recorded over a period of 3 h. The shortest reproducible cycle delay has been determined to be 0.3 s.

**Determination of Standardized *S*(cid)/*N*.** The signal-to-noise (*S*/*N*) ratio of the $^{13}$C photo-CIDNP signals of RCs of *Rb. sphaeroides* WT and R26 measured at 4.7 and 9.4 T with a cycle delay of 4 s[12,13] has been determined. Correcting for the experimental times, the ratio has been found to be 1.0:1.8 in favor of the photo-CIDNP signals obtained at 4.7 T.

**Fitting of Recovery Times $T_R$.** Recovery curves were fitted by a superposition of a fast recovering fraction $p_f$ with recovery time $T_{R,f}$ and a slowly recovering fraction $1 - p_f$ with recovery time $T_{R,s}$. For each fraction the signal-to-noise ratio as a function of repetition time $t_{rep}$ was modeled by eq 7 derived below. Fits were performed by Nelder−Mead simplex minimization of the root-mean-square deviation between experimental and simulated data using a homewritten Matlab program that is available from the authors on request.

**Computation of Polarization Gains and Losses during a Photocycle.** Nuclear polarization gains during a single photocycle were computed by density operator formalism, spin Hamiltonian parameters from literature, and density functional theory computations as described before.[12] The fraction of nuclear polarization lost by coherent spin evolution of the radical pair during a single photocycle was computed by density operator formalism in the same way, substituting the nuclear spin unit operator in the initial density operator by $2\hat{I}_z$. The fraction of nuclear polarization lost due to longitudinal relaxation in the triplet state was computed by eq 11 derived below using estimates for the relaxivity of the electron spin triplet obtained earlier by fits of photo-CIDNP patterns of R26 RCs.[13]

## 3. Theory

**Source and Drain Terms in Photo-CIDNP Buildup Kinetics.** Recovery of the nonequilibrium polarization in photo-CIDNP experiments is due to a buildup process that involves polarization source and drain terms rather than due to straightforward longitudinal relaxation. During each photocycle, new polarization $\Delta p_0$ is generated and a fraction $f_l$ of the existing polarization $p(t)$ is lost. Established theory of polarization buildup in CIDNP and DNP experiments assumes a constant rate of polarization generation (zeroth-order process) and

polarization losses exclusively due to longitudinal relaxation with time constant $T_1$ (first-order process). As a result polarization recovers exponentially with the longitudinal relaxation time $T_1$. In general, the effective $T_1$ is a residence time weighted average of the longitudinal relaxation times of nuclear spins in the diamagnetic ground state and in excited and radical pair states. Due to the short lifetime of the excited and radical pair states, the effective $T_1$ is usually assumed to be equal to $T_1$ in the electronic ground state. In the following we demonstrate that contributions of other electronic states may be significant in solid-state photo-CIDNP of systems with an enhanced triplet lifetime and, perhaps more surprisingly, that there is an additional coherent pathway of polarization loss that does not have the properties of a relaxation process.

We first consider the source term $\Delta p_0$ which in solid-state photo-CIDNP is due to the conversion of electron two-spin order in the spin-correlated radical pair to nuclear polarization by the TSM, DD, and DR mechanisms. As long as $p \ll 1$, this source term does not depend on the existing polarization $p$ that is of the order of $5 \times 10^{-6}$ at thermal equilibrium and smaller than 0.03 for the maximum solid-state photo-CIDNP effects observed to date. The approximation of a polarization-independent source term is thus valid for all solid-state CIDNP experiments reported to date.

The drain term $f_l\, p(t)$ consists of a coherent and an incoherent contribution. (i) The coherent contribution occurs in the TSM and DD mechanisms and is caused by the noncommutation of the nuclear polarization operator $I_z$ with the pseudosecular hyperfine coupling term $B\, S_z I_x$ in the spin Hamiltonian of the radical pair state. Hence, part of the existing nuclear polarization is reconverted to other forms of spin magnetization by coherent spin evolution in the radical pair state. This coherent loss term is roughly proportional to $B^2 = 9 \sin^2\theta \cos^2\theta\, \Delta A^2$, where $\Delta A = A_{zz} - (A_{xx} + A_{yy})/2$ is the $^{13}$C hyperfine coupling anisotropy and $\theta$ is the angle between the magnetic field and the unique axis of the hyperfine coupling tensor. The powder average of the coherent loss term for a macroscopically isotropic sample is thus proportional to $\Delta A^2$. Coherent loss is conceptually different from relaxation processes as it is not caused by stochastic fluctuations of local fields but rather by deterministic spin evolution. It can thus be predicted quantitatively from magnetic parameters of the spin Hamiltonian without any knowledge on molecular dynamics in the system. (ii) The incoherent contribution occurs in the DR mechanism and is caused by enhanced nuclear spin relaxation during the lifetime of the radical pair $\tau_{RP}$ and, for the fraction of RCs that relax to the ground state via the triplet branch, from enhanced relaxation during the lifetime $\tau_T$ of the donor triplet state. This contribution corresponds to a mere residence time weighted averaging of relaxation times of the ground state and triplet state. It also leads to a contribution to the effective $T_1$ that depends on light intensity as the ratio of residence times in the excited and ground state depends on the rate of photon absorption. Due to this contribution $f_l$ also depends on the lifetime of the triplet state and is thus expected to differ between WT and R26 RCs. In the kinetic law the aforementioned source and drain terms have to be multiplied by the rate $k_p$ of photon absorption by the RCs. A further drain term results from nuclear spin longitudinal relaxation in the diamagnetic ground state with time constant $T_1$. The kinetic law in differential form is thus given by

$$\frac{dp(t)}{dt} = k_p \Delta p_0 - f_l k_p p - \frac{p}{T_1} \qquad (1)$$

Integration results in

$$p(t) = p_0 + \frac{k_p \Delta p_0}{f_l k_p + T_1^{-1}}\{1 - \exp[-(f_l k_p + T_1^{-1})t]\} \qquad (2)$$

where $p_0$ is the polarization at $t = 0$. For buildup experiments with a light shutter, $p_0 = p_{th}$ is the thermal equilibrium polarization, while in the context of signal recovery $p_0$ is the polarization left immediately after the NMR experiment. For Hahn echo detection with flip angles of $\pi/2$ and $\pi$, as used in this work, $p_0 = 0$. The maximum polarization gain at infinite recovery time compared to $p_0$ is generally proportional to $\Delta p_0$, which justifies our previous simulations of polarization patterns based on considerations for only a single photocycle.[12,13] The buildup is exponential, just as in the case of recovery of thermal equilibrium polarization. It can thus be characterized by a recovery time $T_R$.

Three buildup regimes can be distinguished. (i) In the linear regime, where $f_l k_p \ll T_1^{-1}$, relaxation in the diamagnetic ground state dominates the polarization loss. Exponential buildup with the same time constant $T_1$ as in recovery of thermal equilibrium polarization is observed, and the maximum polarization gain is given by $k_p \Delta p_0 T_1$, i.e., linear in the photon absorption rate $k_P$. To a good approximation, $\Delta p_0$ is proportional to $B^2$, and thus to $\Delta A^2$, for the TSM[28] and DD mechanism at short radical pair lifetimes. For bacterial RCs, numerical computations of the type introduced in ref 12 yield $\Delta p_0 = (-1.20 \pm 0.17) \times 10^{-5} \Delta A^2$ MHz$^{-2}$ and $(-6.07 \pm 1.88) \times 10^{-5} \Delta A^2$ MHz$^{-2}$ at 4.7 and 9.4 T, respectively. As $\Delta A$ scales with the spin density in the $2p_z$ orbital of the carbon atom in the radical pair state, photo-CIDNP intensities in this regime are roughly proportional to the square of this part of the spin density. Using the total $p$ spin density $\rho_p$ from the DFT computations, our numerical computations give $\Delta p_0 = (-0.216 \pm 0.086)\rho_p^2$ at 4.7 T and $\Delta p_0 = (-0.110 \pm 0.056)\rho_p^2$ at 9.4 T. The signal strength grows linearly with the photon absorption rate $k_p$, i.e., for an optically dilute sample, it grows linearly with light intensity. (ii) In the intermediate-light regime, where $f_l k_p \approx T_1^{-1}$, the buildup is still exponential, but the rise time now depends on the rate of photon absorption, the loss factor $f_l$, and the longitudinal relaxation time $T_1$. The maximum polarization gain also depends on these three parameters. (iii) Finally, in the light-saturation regime, where $f_l k_p \gg T_1^{-1}$, the rise time is $1/f_l k_p$ and the maximum polarization achieves $\Delta p_0/f_l$. It is independent of $k_P$. Furthermore, as $f_l$ is also roughly proportional to $\Delta A^2$, the remarkable prediction ensues that in the light saturation regime the polarization due to the TSM and DD does not depend on the hyperfine coupling in the radical pair state. Note however that even at arbitrarily high light intensity $k_P$ cannot exceed $(\tau_{RP} + \tau_T)^{-1}$. Hence, independently of the available light intensity, the light-saturation regime can only be attained for loss factors $f_l$ above a certain limit and thus only for hyperfine couplings above a certain lower limit. Nevertheless, it can be concluded that under saturation conditions differences between the polarizations of nuclei with different hyperfine couplings are diminished.

In general, $\Delta p_0$ and $f_l$ differ strongly between different nuclei, while $T_1$ differs only slightly and $k_p$ is the same for all nuclei in the same RC. In optically thin samples, $k_p$ is constant across the whole sample and exponential recovery is expected not only for each individual RC but also for the sample as a whole. In optically thick samples, $k_p$ depends on the distance of the RC from entry point of the light beam into the sample and decreases with increasing distance from its maximum value at the entry point to a value close to zero. In this situation recovery is nonexponential in the intermediate and light-saturation regimes. As $f_l$ and $T_1$ are expected to be constant across the sample, the

distribution of recovery times

$$T_R = (f_l k_p + T_1^{-1})^{-1} \quad (3)$$

can be computed by expressing $k_p$ from the photon absorption rate $k_{p,0}$ at the entry point by the Lambert−Beer law

$$k_p = k_{p,0} \exp(-\epsilon x) \quad (4)$$

where $x$ is the distance from the entry point of the light beam and $\epsilon$ is a constant that is proportional to the extinction coefficient. For simplicity we assume that the differential sample volume d$v$ does not vary with $x$. The contribution $p(x)$ of such a differential volume element is then weighted by a factor exp(−$\epsilon x$). For optically dense samples that absorb all incident light, knowledge of $\epsilon$ is not required. The average recovery curve can be computed with good precision by integration over the parameter $\xi = \epsilon x$ from $\xi = 0$ to $\xi = 5$.

**NMR Signal Recovery as a Function of Repetition Time.** Since upon repetition of experimental cycles both signal and noise are accumulated, signal recovery in solid-state photo-CIDNP is most conveniently characterized by measuring the dependence of the signal-to-noise ($S/N$) ratio on the repetition time $t_{rep}$ of the experiment at constant total measurement time $t_{meas}$. At the same time such a measurement provides an experimental value for the optimum repetition time. Assuming that the polarization is completely destroyed by the NMR experiment ($p_0 = 0$), the recovered polarization at time $t_{rep}$ is given by

$$p(t_{rep}) = p_{max}[1 - \exp(-t_{rep}/T_R)] \quad (5)$$

where

$$p_{max} = \frac{k_p \Delta p_0}{f_l k_p + T_1^{-1}} \quad (6)$$

The signal is proportional to $p(t_{rep})$ and to the number of scans, $n = t_{meas}/t_{rep}$, while the noise is proportional to the square root of $n$ and thus to $t_{rep}^{-1/2}$. Hence, the signal-to-noise ratio as a function of $t_{rep}$ is given by

$$\frac{S}{N}(t_{rep}) = C t_{rep}^{-1/2}\left[1 - \exp\left(-\frac{t_{rep}}{T_R}\right)\right] \quad (7)$$

where $C$ is a constant factor that is proportional to $p_{max}$. For optically thick samples, $C$ is also proportional to exp(−$\epsilon x$), so that integration over $x$ is required. In this integration the dependence of $k_p$ on $x$, eq 4, and thus of $T_R$ on $x$ needs to be considered. The recovery time $T_R$ can be obtained by fitting eq 7, or the corresponding integral over $x$, to the measured data. By letting the first derivative of eq 7 to zero, we find as an expression for the optimum repetition time

$$\exp(-t_{rep,opt}/T_R) = 1 + 2t_{rep,opt}/T_R \quad (8)$$

Numerical evaluation of this expression yields

$$t_{rep,opt} \approx 1.2564 T_R \quad (9)$$

**Estimate of Polarization Loss Factors.** Outside the linear regime the recovery time $T_R$ differs from $T_1$ and depends on the loss factor $f_l$ as well as the rate of photon absorption $k_p$. For the rate of photon absorption an upper limit of 20−100 s$^{-1}$ has been estimated previously from the measured light power[21] and a lower limit of ten times the rate of longitudinal relaxation, corresponding to 0.5 s$^{-1}$, has been derived from experimental polarizations.[12] The coherent loss factor $f_{l,c}$ can be predicted by numerical computations based on the density operator formalism as they were used before to predict $\Delta p_0$.[12,13] The initial density operator in the fictitious spin basis for the $ST_0$ manifold,[18] which is $\hat{1}/2 - \hat{S}_x$ in the computations of $\Delta p_0$, is replaced by $\hat{I}_z - 2\hat{S}_x\hat{I}_z$, and $f_{l,c}$ is computed from the expectation value $\langle I_z \rangle_{dia}$ in the diamagnetic ground state after decay of the radical pair and donor triplet as

$$f_{l,c} = 1 - \langle I_z \rangle_{dia} \quad (10)$$

Such computations were performed at magnetic fields $B_0$ of 4.7 and 9.4 T for the nuclei C-Φ2, C-Φ5, and C-Φ20 of the bacteriopheophytin acceptor as well as C-M11, C-M14, C-L14, C-L16, and C-L19 of the special pair donor, using the nomenclature introduced in ref 12. We find $f_{l,c} = (6.72 \pm 0.81) \times 10^{-5} \Delta A^2$ MHz$^{-2}$ and $f_{l,c} = (2.64 \pm 0.46) \times 10^{-5} \Delta A^2$ MHz$^{-2}$ at $B_0 = 4.7$ and 9.4 T, respectively. For hyperfine anisotropies $\Delta A$ between 5 and 15 MHz that are typical for clearly visible signals, this corresponds to loss factors between $2 \times 10^{-3}$ and $1 \times 10^{-2}$ at $B_0 = 4.7$ T and between $8 \times 10^{-4}$ and $4 \times 10^{-3}$ at 9.4 T. For a $^{13}$C longitudinal relaxation time of $T_1 = 20$ s and a photon absorption rate $k_p = 50$ s$^{-1}$, eq 3 thus predicts recovery times $T_R$ between 1.8 and 6.7 s at 4.7 T and between 4 and 11 s at 9.4 T, if incoherent losses are negligible. For the lower limit of $k_p = 0.5$ s$^{-1}$ the recovery time is still slightly decreased to 18.2 s at $f_l = 1 \times 10^{-2}$. Hence, we generally expect that recovery is not in the linear regime.

Incoherent loss factors are given by

$$f_{l,i} = 1 - \exp(-C_{dd} \Delta A^2 \tau_T) \quad (11)$$

where $C_{dd}$ is a field-dependent parameter and $\Delta A$ is now the hyperfine anisotropy of the $^{13}$C nucleus in the triplet state. In previous work we approximated $\Delta A$ by the corresponding value for the radical pair state and found $C_{dd} = 4 \times 10^{-11}$ s at 4.7 T and $C_{dd} = 6 \times 10^{-11}$ s at 9.4 T by fitting the polarization patterns in photo-CIDNP spectra of R26 RCs.[13] On this level of theory, significant incoherent losses are expected only for $^{13}$C nuclei in the special pair donor. For the WT RCs with $\tau_T =$ 100 ns incoherent loss factors according to eq 11 range between $3 \times 10^{-4}$ and $7 \times 10^{-4}$ at 4.7 T for strongly coupled $^{13}$C and are by a factor of 1.5 larger at 9.4 T. They are smaller than the coherent loss factors for the same atom by about a factor of 15 at 4.7 T and about a factor of 4 at 9.4 T. In WT RCs incoherent loss thus does not play a significant role. This is dramatically different for R26 RCs with a triplet lifetime $\tau_T = 100$ $\mu$s. In this situation incoherent loss factors exceed coherent loss factors by a factor of about 50 at 4.7 T and a factor of about 170 at 9.4 T and are as large as 0.2−0.6 for strongly coupled $^{13}$C. Even at a photon absorption rate $k_{p,0}$ of only 0.5 s$^{-1}$, a loss factor of 0.6 leads to a signal recovery time $T_R$ as low as 3 s at a longitudinal relaxation time $T_1 = 20$ s. To conclude with the estimate of loss factors, we note that the total loss factor is given by

$$f_l = 1 - (1 - f_{l,c})(1 - f_{l,i}) = f_{l,c} + f_{l,i} - f_{l,c} f_{l,i} \quad (12)$$

## 4. Results

**Photo-CIDNP MAS NMR on Photosynthetic RCs.** Figure 3 demonstrates the effect of photo-CIDNP in various photosynthetic RCs under illumination with continuous white light as detected with $^{13}$C MAS NMR. Spectrum 3A has been obtained from solubilized RCs of *Rb. sphaeroides* R26 in the

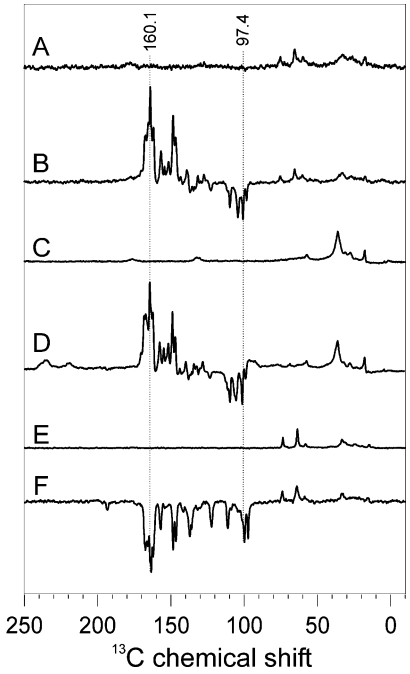


**Figure 3.** $^{13}$C MAS NMR spectra of the investigated samples: bacterial R26 RCs in the dark (A) and under illumination (B), bacterial R26 RCs mounted on glass disks in the dark (C) and under illumination (D), as well as bacterial WT RCs in the dark (E) and under illumination (F). Dotted lines indicate the frequency of signals used for analysis of relaxation kinetics. All spectra were measured at 4.7 T, $T = 235$ K, a MAS rotational frequency of 8 kHz, a cycle delay of 4 s, and a experimental time of ~12 h.

dark. The spectrum shows solely normal features of a protein, especially below 70 ppm and in the carbonyl region around 180 ppm. Upon illumination with continuous white light, strong enhanced absorptive (positive) and emissive (negative) signals appear (spectrum 3B). These signals originate from the aromatic carbons of the bacteriochlorophyll (BChl) and bacteriopheophytin (BPhe) involved in the formation of the radical pair.[6,13] The negative signals around 100 ppm originate from the methine carbons of the macrocycles. Spectra 3C and 3D originate from R26 RCs mounted on glass disks. Additional signals occur from the lipids of the membrane. The photo-CIDNP signature is quite similar to that of solubilized RCs (spectrum 3B); however, the optical properties of such samples are different due to the dilution by glass layers allowing for deeper penetration of the light into the rotor. RCs of *Rb. sphaeroides* WT (spectra 3E and 3F) show under light a completely emissive photo-CIDNP signature.[12] The difference in signature is due to the long triplet lifetime of the donor allowing for the DR mechanism in R26 RCs.[13]

**Recovery Experiments on Photosynthetic Reaction Centers.** Figure 4 shows the ratio of the photo-CIDNP signal at 160.1 ppm of R26 RCs to the noise level ($S$(cid)/$N$) for different cycle delays for 9.4 (trace A) and 4.7 T (trace B). The values are standardized by setting the value measured at 9.4 T and a cycle delay of 4 s to unity. At 9.4 T, the optimum $S$(cid)/$N$ is observed with cycle delays between 4 and 5 s. From kinetic analysis of trace A, a recovery time of 4.1 s is obtained. On a logarithmic scale, the rise and the decay appear to be almost linear and form a quite symmetric shape. With a cycle delay of 4 s, the $S$(cid)/$N$ at 4.7 T (trace B) is a factor of 1.8 better than that obtained at 9.4 T. At 4.7 T, the optimum standardized $S$(cid)/$N$ is found at 2.0 s with a value of 2.1 units. The shape of the curve, however, does not appear to be symmetric. On a logarithmic scale, a linear decay is observed on the right wing,

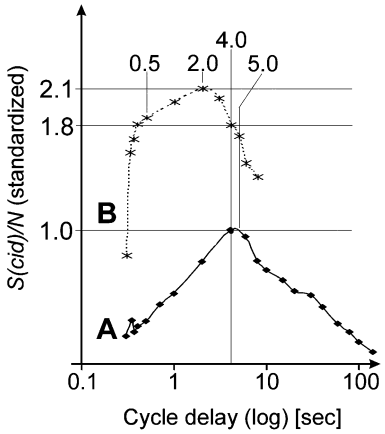


**Figure 4.** Dependence of the photo-CIDNP signal intensity on the cycle delay time at 9.4 (A) and 4.7 T (B), obtained for the signal at 160.1 ppm as observed in the spectrum of RC of *Rb. sphaeroides* R26 (spectrum 3B). The photo-CIDNP signal intensity is expressed relative to the noise level ($S$(cid)/$N$). Each data point represents the standardized $S$(cid)/$N$ of a photo-CIDNP MAS NMR spectrum obtained in 4 h. For the standardization, the $S$(cid)/$N$ of the photo-CIDNP MAS NMR spectrum measured a 9.4 T and a cycle delay of 4 s was set to unity. Under identical conditions, the photo-CIDNP MAS NMR spectrum obtained at 4.7 T reveals a 1.8 times better $S$(cid)/$N$ ratio than at 9.4 T.

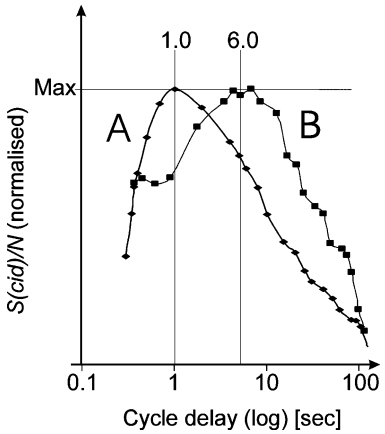


**Figure 5.** Dependence of the photo-CIDNP signal intensity on the cycle delay time obtained at 4.7 T for the signal 160.1 ppm in the spectrum of RC of (A) *Rb. sphaeroides* R26 (spectrum 3D) and (B) WT (spectrum 3F). The photo-CIDNP signal intensity is expressed relative to the noise level ($S$(cid)/$N$). Each data point represents the $S$(cid)/$N$ of a photo-CIDNP MAS NMR spectrum obtained in 4 h. For normalization, the strongest ($S$(cid)/$N$) values were set to unity.

while at the left wing a second optimum may occur. Furthermore, there is a very sharp increase between 0.3 and 0.5 s. These observations may indicate the occurrence of a fast second recovery channel. Since the photo-CIDNP activity of bacterial RCs is at a factor of 10 higher at 4.7 T compared to 9.4 T,[12,13] it is reasonable to assume that such a recovery channel is due to high photo-CIDNP activity. Using a R26 sample mounted on glass disks allows for increase of light penetration into the inner parts of the rotor from which a stronger NMR signal is obtained. Hence, it is expected that these samples show an increase of the photo-CIDNP induced recovery channel. In fact, under these conditions, a strong increase of the fast relaxation channel occurs at 4.7 T (Figure 5, trace A). This asymmetric curve is sharply rising at about 0.3−0.5 s and has a maximum at 1.0 s.

In order to test which of the possible polarization drain terms drives the fast recovery channel, experiments have been performed using WT RCs, having a triplet lifetime of $\tau_R = 100$

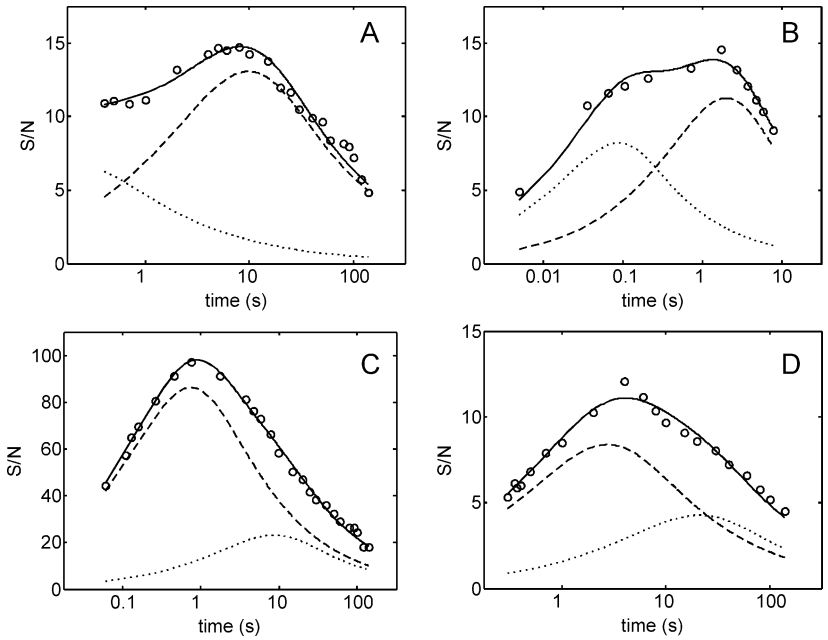


**Figure 6.** Best fits of the recovery kinetics by a two-component model: (A) *Rb. sphaeroides* WT at 4.7 T; (B) R26 at 4.7 T; (C) R26 with glass disks at 4.7 T; (D) R26 at 9.4 T. Solid lines correspond to the sum of both components, dashed lines to the major component, and dotted lines to the minor component.

**TABLE 1: Parameters Obtained from Kinetic Fitting**

| | RC WT 4.7 T | RC R26 4.7 T | RC R26 4.7 T, glass disks | RC R26 9.4 T |
|---|---|---|---|---|
| fast recovery time $T_{Rf}$ (s) | 0.01 | 0.04 | 0.54 | 2.53 |
| slow recovery time $T_{Rs}$ (s) | 7.88 | 1.4 | 5.49 | 31.01 |
| photon rate $k_{p,0}$ ($s^{-1}$) | 15 | 15 | 15 | 10 |
| relaxation time $T_1$ (s) | 17 | 17 | 17 | 17 |
| loss factor $f_l$ (minor) | 0.68 | $\leq 1$ | | |
| loss factor $f_l$ (major) | $7 \times 10^{-3}$ | 0.04 | 0.18 (100%) | 0.064 (100%) |

ns, which is by a factor of 1000 shorter than the triplet lifetime of R26 RCs (Figure 5, trace B). The optimum cycle delay is at 6 s, suggesting that in WT samples the fast recovery path is not activated under current experimental conditions. Hence, the incoherent loss term due to nuclear spin longitudinal relaxation in the triplet state appears to be responsible for the fast recovery.

**Analysis of the Recovery Kinetics.** On the basis of the theory that was outlined above, we have attempted to fit the experimental data on signal recovery. Recovery times were first determined based on eq 7 without considering the known value for $T_1$ (first two lines of Table 1). The data were then fitted again using eq 3 with known values of $T_1$ and $k_p$ as a constraint on $T_R$ and assuming optically dense samples. Fit quality did not significantly deteriorate. Note that only the product of $k_{p,0}$ and $f_l$ can be determined. It turned out that in none of the four cases was a single set of parameters ($T_1$, $k_{p,0}$, $f_l$) sufficient to obtain good fits. In all cases good fits were obtained with two components with different loss factors but the same value of $T_1 = 17$ s (Figure 6). This value for the longitudinal relaxation time corresponds to the average experimental value determined before.[6] To tentatively separate the maximum photon absorption rate $k_{p,0}$ and the loss factors, we assumed that the loss factor of the major component of WT RCs at 4.7 T (dashed line in Figure 6a) agrees with the theoretical value of the coherent loss factor of $f_{l,c} = 7 \times 10^{-3}$, averaged over nuclei C-L14, C-L19, and C-Φ5 that contribute to the signals marked in Figure 2. We thus find $k_{p,0} = 15\ s^{-1}$, which is close to the range of 20−100 $s^{-1}$ estimated from available light power.[21] Hence, we may discuss all further results under the assumptions $T_1 = 17$ s and $k_{p,0} = 15\ s^{-1}$, except for the data at 9.4 T, where light intensity is by a factor of $^2/_3$ smaller in our setup, so that we use $k_{p,0} = 10\ s^{-1}$. The minor recovery component of WT RCs (dotted line in Figure 6a) corresponds to faster recovery with a loss factor as high as 0.68. A component with a large loss factor would ensue if paramagnetic byproducts were accumulated in fractions of the sample, as nuclear spin relaxation is enhanced in the neighborhood of paramagnetic centers. Trapping of a fraction of RCs in paramagnetic states has been observed for the WT in the presence of the secondary quinone acceptor[29] and for the R26 strain also with a prereduced secondary acceptor, corresponding more closely to the situation in our samples.[30,31]

Indeed, we also find a minor very fast recovering component in the R26 RCs at 4.7 T MHz (dotted line in Figure 6b), which corresponds to a loss factor close to unity. The major component has a loss factor of 0.04, which is significantly smaller than the expected incoherent loss factor. The very fast recovering component is not observed for the optically more dilute sample of R26 RCs containing glass disks at the same field (Figure 6c), which suggests that the trapping of paramagnetic states is enhanced by the larger local heat dissipation that occurs in the optically undiluted R26 sample. Indeed, recovery of the R26 sample prepared containing glass disks is strongly dominated by a component with a loss factor of 0.18, which is reasonably close to the theoretically predicted *average* incoherent loss factor of all observed nuclei. The loss factor of this major component does not differ significantly between the absorptive signal at 160.1 ppm and the emissive signal at 97.4 ppm. The minor component has a loss factor indistinguishable from zero. As this loss factor is significantly smaller than the predicted

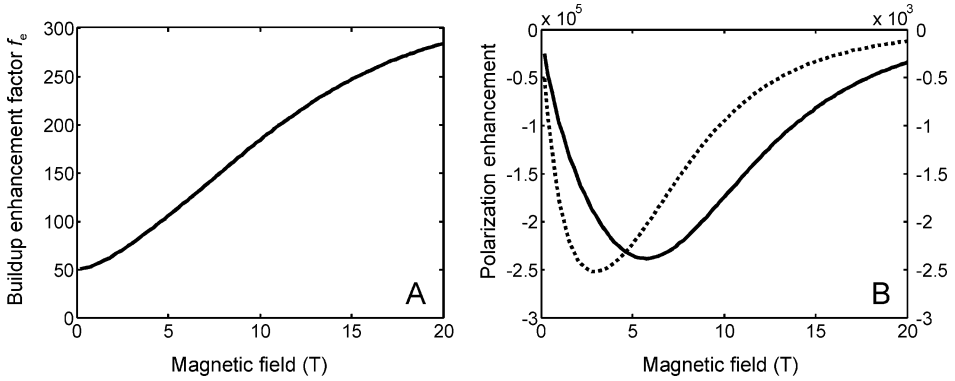


**Figure 7.** Influence of buildup kinetics on the magnetic field dependence of photo-CIDNP. Data were simulated for the donor $^{13}$C nucleus C-L19 in WT RCs assuming a field-independent longitudinal relaxation time $T_1 = 17$ s and a photon absorption rate $k_{p,0} = 20$ s$^{-1}$. (A) Magnetic field dependence of the buildup enhancement factor $f_e$, eq 14. (B) Magnetic field dependence of the polarization enhancement relative to thermal equilibrium polarization for a single photocycle (dotted line, right scale) and during continuous illumination (solid line, left scale).

coherent loss factor, a fraction of the $^{13}$C nuclei might not be polarized directly by photocycles but rather by spin diffusion.

The recovery kinetics of R26 RCs at 9.4 T is of the same type as for the R26 RCs containing glass disks at 4.7 T, although the time scale is slower. In fact, the loss factor of 0.064 is similar to the one observed for the same R26 sample at 4.7 T. The main difference is due to the lack of the very fast recovering component at 9.4 T and the presence of a very slow recovering component with a loss factor close to zero. We cannot preclude the existence of such a slow recovering component for the same sample at 4.7 T, as it contributes most significantly at repetition times longer than 10 s where we do not have data at 4.7 T for the R26 sample without glass disks. However, for the WT sample, we can preclude the presence of such a component.

## 5. Discussion

***T*$_1$ Relaxation of Aromatic Carbons.** Measuring the signal decay in nanosecond-flash photo-CIDNP MAS NMR experiments, recently we have examined the $T_1$ values of six selectively $^{13}$C-labeled aromatic carbons of the BChl cofactors of bacterial RCs of *Rb. sphaeroides* WT at 4.7 T.[6] The measurements revealed $T_1$ values between 13.7 and 22.4 s with an average of 17 s. Hence, $^{13}$C atoms of the aromatic cofactors in photosynthetic RCs show relaxation properties in the expected range for aromatic carbons. The $T_1$ times of the carbons of the aromatic cofactors in both RCs, WT and R26, are expected to be similar, as the presence of a remote carotene should not affect the nuclear relaxation times at the special pair cofactors. Our assumption of a uniform $T_1$ of about 17 s in the modeling of all four recovery curves can thus be considered as valid for a semiquantitative analysis.

**Comparison with Earlier Studies on Photo-CIDNP Buildup.** In a photo-CIDNP buildup study at 9.4 T based on shutter experiments on bacterial RCs of *Rb. sphaeroides* R26, the full polarization was reached after a period of illumination of 20 s.[6,32] For the signal at a chemical shift of 161 ppm, first-order kinetics fit gave a time constant $k = 0.27$ s$^{-1}$, corresponding to a time constant of 3.7 s. This buildup is thus significantly faster than longitudinal relaxation. A fit of our recovery data of R26 RCs at the same field by a superposition of two components reveals recovery times of 2.5 s for the faster recovering component. This is in reasonable agreement with the buildup data. The apparently longer buildup time probably results from the impossibility to separate a fast and slow component in these data. Indeed a single-component fit of the present recovery data gives an average recovery time of 4.2 s but is significantly worse than the two-component fit. Recovery experiments thus provide a more detailed picture of the sample.

In an earlier theoretical study buildup kinetics was simulated numerically taking into account only the DD mechanism and neglecting variations of the photon absorption rate across the sample.[19] The numerical results, displayed in Figure 6c of that reference, can be fitted almost perfectly by the simplified expression

$$p(t) = p_{max}[1 - \exp(-t/T_R)] \qquad (13)$$

with a recovery time $T_R = 4.9$ s. As the authors assumed $T_1 = 10$ s and $k_p = 50$ s$^{-1}$, this corresponds to a loss factor $f_l = 2 \times 10^{-3}$. This agrees with expectations for a model that considers only a DD mechanism but differs considerably from the actual loss factors for R26 RCs that include incoherent losses.

**Mechanism of Fast Recovery.** Signal recovery in solid-state photo-CIDNP experiments is significantly faster than expected from the longitudinal relaxation time $T_1$ of the nuclear spins in the absence of light. For the major signal components in all four samples, this faster recovery could be traced back to polarization losses during the photocycle. Minor signal components in R26 RCs at 9.4 T and in R26 RCs mounted on glass disks at 4.7 T recover with the longitudinal relaxation time. Such behavior is expected for inactive RCs that do not undergo photocycles but are polarized due to spin diffusion. Minor signal components in R26 and WT RCs at 4.7 T exhibit very fast recovery, with rates that correspond to an almost complete loss of the existing polarization before or during the next photocycle. This behavior may result from the presence of persistent paramagnetic species in the neighborhood that lead to enhanced longitudinal relaxation.

The recovery kinetics of the major component in WT RCs at 4.7 T is consistent with the theory outlined above, using the known longitudinal relaxation time and a coherent loss factor predicted for reconversion of nuclear polarization to other magnetization terms due to spin evolution during the lifetime of the radical pair. A fit to the experimental data then yields a maximum photon absorption rate of 15 s$^{-1}$. This is in reasonable agreement with estimates of 20−100 s$^{-1}$ based on the available light intensity, considering that the computation of the loss factors involves some uncertainty in the magnetic parameters of the radical pair.

Loss factors for the major component in concentrated samples of R26 RCs at both 4.7 and 9.4 T are higher than those for WT RCs at 4.7 T, in agreement with the expectation of additional incoherent losses in R26 RCs due to enhanced nuclear longi-

tudinal relaxation during the lifetime of the special pair triplet state. However, the loss factors are still significantly smaller than those expected from theory. They correspond to longer recovery times than predicted. The agreement with theoretical predictions is better, yet not perfect, for R26 RCs prepared with a stack of glass disks, corresponding to an effective dilution of the sample. In the latter sample, the recovery time of the major component is as short as 0.54 s, by a factor of about 30 shorter than $T_1$.

Recovery of the emissive signals assigned to the bacteriopheophytin acceptor and of the absorptive signals assigned to the special donor in R26 RCs is not significantly different (data not shown). This is in contradiction with the simple theory outlined above, which predicts that the incoherent losses occur only for nuclei in the donor chromophores, while acceptor nuclei should exhibit the same recovery behavior as in WT RCs. Experimental data suggest that the recovery kinetics is uniform with an average incoherent loss factor. With respect to recovery, all nuclei of the RC thus seem to behave as a single spin bath. However, these nuclei keep their individual polarizations which may even differ in sign, which contradicts the idea of a single spin bath. Further work is required to understand this phenomenon.

**Maximum Polarization and Signal-to-Noise Enhancement.** The detection of RC fractions with different photo-CIDNP recovery kinetics is significant for an estimate of the maximum polarization enhancement that is possible with this technique. The best estimates obtained to date[12,13] were averages over the whole sample, not taking into account the variation of light intensity across the sample. Furthermore, the existence of RCs that either do not take part in photocycles or are in trapped paramagnetic states, which precludes significant polarization buildup in subsequent photocycles, has not been considered. The kinetic parameters obtained in this work, together with eq 2, allow for the computation of enhancement factors

$$f_e = \frac{k_{p,0}}{f_l k_{p,0} + T_1^{-1}} \tag{14}$$

that quantify the maximum extent of accumulation of nuclear polarization in subsequent photocycles. Approximate enhancement factors at a magnetic field of 4.7 T are $f_e \approx 90$ for WT RCs, $f_e \approx 23$ for undiluted R26 RCs, and $f_e \approx 5.5$ for R26 RCs mounted on glass disks. As the polarization gain during a single photocycle is predicted to be up to 1000 times larger than thermal equilibrium polarization for WT RCs,[12] a maximum enhancement of 90000 is expected. The average enhancement is therefore almost an order of magnitude larger than that observed to date. The missing enhancement is probably due to the use of optically dense samples, which suggests that dilution of the sample leads to smaller signal losses than previously expected.

In the absence of incoherent losses the enhancement factor according to eq 14 increases with increasing magnetic field (Figure 7A) as the coherent loss factor decreases. This causes a shift in the optimum field for photo-CIDNP experiments for an experiment with continuous illumination (solid line in Figure 7B) compared to the expectations for a single photocycle (dotted line). For R26 RCs, having significant incoherent losses, the field dependence of the loss factor and thus also of the enhancement factor is related to the relative field dependences of the longitudinal relaxation times of the nuclear spin in the triplet state and in the diamagnetic ground state. Currently we have no experimental data on the field dependence of the relaxation times that are sufficiently precise for predictions. However, we expect that in this case only minor shifts of the optimum field will occur.

The gain in $S/N$ obtained by photo-CIDNP experiments is determined not only by the polarization gain $\Delta p_0$ during a single photocycle and the enhancement factor $f_e$ but also by the opportunity to repeat the experiment faster than a standard NMR experiment on the same sample. According to eqs 3 and 9, the optimum repetition rate scales as

$$k_{rep,opt} = (f_l k_p + T_1^{-1})/1.2564 \tag{15}$$

As the $S/N$ increases with the square root of $k_{rep}$, eqs 14 and 15 imply a scaling as

$$\frac{S}{N} \propto \frac{k_{p,0}}{\sqrt{f_l k_{p,0} + T_1^{-1}}} \tag{16}$$

Assuming similar polarization gain during a single photocycle, the optimum $S/N$ for undiluted R26 RCs is thus about half that for WT RCs, although the enhancement factor $f_e$ is by a factor of 4 smaller.

## 6. Conclusions

The recovery of the NMR signal after a solid-state photo-CIDNP experiment on photosynthetical RCs was found to be up to a factor of 30 faster than expected from the longitudinal relaxation time, corresponding to an additional signal-to-noise enhancement by a factor of more than 5 for an optimized repetition rate. This faster recovery is a consequence of additional decay channels for the nuclear polarization during the photocycle. These additional decay channels are the conversion of nuclear polarization to other magnetization during coherent spin evolution in the radical pair state and the incoherent loss of nuclear polarization due to enhanced nuclear relaxation during the lifetime of the donor triplet state. The coherent loss term creates a shortening of the recovery time by a factor of about 3, while incoherent loss contributes a factor of about 10. The faster permissible repetition of the experiment thus comes at the expense of a smaller extent of accumulation of polarization from subsequent photocycles. Our results are in agreement with theoretical predictions for enhanced signal recovery, except for the fact that donor and acceptor nuclei in R26 RCs appear to recover as a single spin bath in the experiments, while theory predicts faster recovery of the donor nuclei and slower recovery of the acceptor nuclei than observed.

The knowledge of the spin-dynamical processes allows for further optimization of the sensitivity of solid-state photo-CIDNP experiments as well as for development of a strategy to drive solid-state NMR beyond the $T_1$ limit. In addition, the measurement of the recovery kinetics has turned out to be a sensitive experiment for the detection of different fractions of photosynthetic RCs in a sample. Nonfunctional RCs appear to recover polarization with the longitudinal relaxation time, while RCs in trapped paramagnetic states or in the neighborhood of trapped paramagnetic states recover their polarization very fast. The occurrence of such a very fast recovering component appears to depend on the optical density of the sample. Recovery kinetics data thus provide a convenient means for detecting photochemical side reactions.

**Acknowledgment.** Professor C. Glaubitz is acknowledged for helpful discussions. J.M. thanks Professor H. J. M. de Groot for continuous support. C. Erkelens, F. Lefeber, and J. Hollander

are acknowledged for support during various stages of the experiments. The authors thank A. de Wit and W. van der Meer for their help in sample preparation. This work has been financially supported by the Volkswagen-Stiftung (I/78010) as well as by The Netherlands Organization for Scientific Research (NWO) through Jonge Chemici award (700.50.521), an Open competition grant (700.50.004), and a Vidi grant (700.53.423) to J.M.

## References and Notes

(1) Hall, D. A.; Maus, D. C.; Gerfen, G. J.; Inati, S. J.; Becerra, L. R.; Dahlquist, F. W.; Griffin, R. G. *Science* **1997**, *276*, 930−932.

(2) Rosay, M.; Zeri, A. C.; Astrof, N. S.; Opella, S. J.; Herzfeld, J.; Griffin, R. G. *J. Am. Chem. Soc.* **2001**, *123*, 1010−1011.

(3) Suter, D.; Mlynek, J. *Adv. Magn. Opt. Reson.* **1991**, *16*, 1−83.

(4) Tycko, R.; Reimer, J. A. *J. Phys. Chem.* **1996**, *100*, 13240−13250.

(5) Jeschke, G.; Matysik, J. *Chem. Phys.* **2003**, *294*, 239−255.

(6) Daviso, E.; Jeschke, G.; Matysik, J. In *Biophysical Techniques in Photosynthesis II*; Aartsma, T. J., Matysik, J., Eds.; Springer: Dordrecht, The Netherlands, 2007; pp 385−399.

(7) Bloch, F. *Phys. Rev.* **1946**, *70*, 460−474.

(8) Pervushin, K.; Vogeli, B.; Eletsky, A. *J. Am. Chem. Soc.* **2002**, *124*, 12898−12902.

(9) Schanda, P.; Brutscher, B. *J. Am. Chem. Soc.* **2005**, *127*, 8014−8015.

(10) Klimke, K.; Parkinson, M.; Piel, C.; Kaminsky, W.; Spiess, H. W.; Wilhelm, M. *Macromol. Chem. Phys.* **2006**, *207*, 382−395.

(11) Zysmilich, M. G.; McDermott, A. *J. Am. Chem. Soc.* **1994**, *116*, 8362−8363.

(12) Prakash, S.; Alia; Gast, P.; de Groot, H. J. M.; Jeschke, G.; Matysik, J. *J. Am. Chem. Soc.* **2005**, *127*, 14290−14298.

(13) Prakash, S.; Alia; Gast, P.; de Groot, H. J. M.; Matysik, J.; Jeschke, G. *J. Am. Chem. Soc.* **2006**, *128*, 12794−12799.

(14) Hoff, A. J.; Deisenhofer, J. *Phys. Rep.* **1997**, *287*, 2−247.

(15) Lendzian, F.; Huber, M.; Isaacson, R. A.; Endeward, B.; Plato, M.; Bönigk, B.; Möbius, K.; Lubitz, W.; Feher, G. *Biochim. Biophys. Acta* **1993**, *1183*, 139−160.

(16) Matysik, J.; Alia; Gast, P.; van Gorkom, H. J.; Hoff, A. J.; de Groot, H. J. M. *Proc. Natl. Acad. Sci. U.S.A.* **2000**, *97*, 9865−9870.

(17) Diller, A.; Alia; Roy, E.; Gast, P.; van Gorkom, H. J.; Zaanen, J.; de Groot, H. J. M.; Glaubitz, C.; Matysik, J. *Photosynth. Res.* **2005**, *84*, 303−308.

(18) Jeschke, G. *J. Chem. Phys.* **1997**, *106*, 10072−10086.

(19) Polenova, T.; McDermott, A. E. *J. Phys. Chem. B* **1999**, *103*, 535−548.

(20) Goldstein, R. A.; Boxer, S. G. *Biophys. J.* **1987**, *51*, 937−946.

(21) McDermott, A.; Zysmilich, M. G.; Polenova, T. *Solid State Nucl. Magn. Reson.* **1998**, *11*, 21−47.

(22) Feher, D.; Okamura, M. Y. *The Photosynthetic Bacteria;* Clayton, R. K., Sistrom, W., Ed.; Plenum Press: New York, 1978.

(23) Okamura, M. Y.; Isaacson, R. A.; Feher, G. *Proc. Natl. Acad. Sci. U.S.A.* **1975**, *72*, 3491−3495.

(24) Glaubitz, C.; Watts, A. *J. Magn. Reson.* **1998**, *130*, 305−316.

(25) Lopez, J. J.; Mason, A. J.; Kaiser, C.; Glaubitz, C. *J. Biomol. NMR* **2007**, *37*, 97−111.

(26) Bennett, A. E.; Rienstra, C. M.; Auger, M.; Lakshmi, K. V.; Griffin, R. G. *J. Chem. Phys.* **1995**, *103*, 6951−6958.

(27) Fischer, M. R.; de Groot, H. J. M.; Raap, J.; Winkel, C.; Hoff, A. J.; Lugtenburg, J. *Biochemistry* **1992**, *31*, 11038−11049.

(28) Jeschke, G. *J. Am. Chem. Soc.* **1998**, *120*, 4425−4429.

(29) van Mourik, F.; Reus, M.; Holzwarth, A. R. *Biochim. Biophys. Acta* **2001**, *1504*, 311−318.

(30) Schenck, C. C.; Parson, W. W.; Holten, D.; Windsor, M. W. *Biochim. Biophys. Acta* **1981**, *635*, 383−392.

(31) Egorova-Zachernyuk, T. A.; Remy, A.; Shkuropatov, A. Y.; Gast, P.; Hoff, A. J.; Gerwert, K.; de Groot, H. J. M. *Vib. Spectrosc.* **1999**, *19*, 347−352.

(32) Prakash, S. Photo-CIDNP studies on reaction centres of *Rhodobacter sphaeroides*, Leiden University, 2006, https://openaccess.leidenuniv.nl/dspace/handle/1887/4555.